

Detecting periodic time scales in temporal networks

Elsa Andres¹

Alain Barrat²

Márton Karsai^{1,3,*}

¹*Central European University, Quellenstraße 51, 1100 Vienna, Austria*

²*Aix Marseille Univ, Université de Toulon, CNRS, CPT, Turing Center for Living Systems, Marseille, France*

³*Alfréd Rényi Institute of Mathematics, Budapest, Reáltanoda utca 13-15, 1053 Hungary*

**Corresponding author: mkarsai@ceu.edu*

Abstract

Temporal networks are commonly used to represent dynamical complex systems like social networks, simultaneous firing of neurons, human mobility or public transportation. Their dynamics may evolve on multiple time scales characterising for instance periodic activity patterns or structural changes. The detection of these time scales can be challenging from the direct observation of simple dynamical network properties like the activity of nodes or the density of links. Here we propose two new methods, which rely on already established static representations of temporal networks, namely supra-adjacency matrices and temporal event graphs. We define dissimilarity metrics extracted from these representations and compute their Fourier Transform to effectively identify dominant periodic time scales characterising the original temporal network. We demonstrate our methods using synthetic and real-world data sets describing various kinds of temporal networks. We find that while in all cases the two methods outperform the reference measures, the supra-adjacency based method identifies more easily periodic changes in network density, while the temporal event graph based method is better suited to detect periodic changes in the group structure of the network. Our methodology may provide insights into different phenomena occurring at multiple time-scales in systems represented by temporal networks. Temporal networks, Fourier transform

1 Introduction

Many complex systems, commonly described as networks, are evolving dynamically as their elements and the interactions between them are subject to changes in time. The recent availability of temporally resolved network data sets has stimulated the emergence of the new field of temporal networks [1, 2, 3], which has been useful to describe a wide range of phenomena, from human behavior [4, 5, 6] to biological and ecological systems [7, 8] or public transportation [9, 10]. The temporal network representation provides an effective tool to investigate the structure and dynamics of these systems, as well as the potential dynamical processes occurring on top of them [11, 1]. In particular, this representation goes beyond the conventional static description of networks [12], as it keeps track of the temporal order of successive interactions between elements. This allows for instance to identify notions of potential causality through the definition of temporal paths between nodes, i.e., series of successive interactions along which information can be transmitted [13, 14].

Temporal networks present different time-dependent properties at different structural scales. For instance, single nodes can be characterised by their instantaneous degree (number of neighbors at a given time) or other instantaneous centrality measures, which may vary as a function of time [15, 12, 16, 3]. Links are also temporal objects: connections between nodes appear and disappear, often following bursty and correlated dynamics, as well as circadian patterns, which are all typical of human dynamics [17, 18, 19]. At mesoscopic scales, temporal networks can exhibit temporal motifs [20, 21, 22], communities [23], core-periphery [24, 25] or other cohesive structures and hierarchies

[26, 27]. These various dynamical properties may evolve at different time scales [28], including overall changes between global states at the macroscopic level [29, 30, 25]. In particular, periodic variations can emerge, e.g. driven by the circadian fluctuations of human behaviour [19, 31], regular scheduling in different contexts like in transportation or schools, or the repetition of metabolic reactions in biological systems [32]. Interesting relevant examples of such variations are given by changes in the connection density in the network, or in the way nodes form and dissolve groups or communities. For example, the number and structure of social interactions vary due to daily rhythms and schedules in contexts such as workplaces, scheduled social gathering or in schools, where students interact within a class during lectures, but also with other classes during breaks [33, 31]. The identification of the temporal scales of periodic variations in a temporal network is an important step for the characterization and understanding of the system under investigation. However, their measure represents a challenge as they co-appear with other arbitrary non-periodic temporal scales, which appear as noise and hinder the possibility to detect the periodic behaviour by simply following the temporal evolution of simple network summary measures.

Some recent works have addressed the detection of relevant temporal scales in temporal networks, e.g. by optimizing the overlap between the sets of events on consecutive time intervals [34] or by searching for the precise recurrence of connections between nodes in different time windows [35]. Another approach consists in defining the correlation between instantaneous adjacency matrices of the temporal graph [36]. Finally, computing a whole similarity matrix between all pairs of timestamps can make it possible to detect states in which the network structure remains stable [30, 29, 25], but this method requires rather heavy computations.

Here, we contribute to this endeavour by defining a new method to measure the periodic time scales of temporal networks. Given a temporal network as input, we first divide it into temporal sub-networks using successive sliding windows. We then use lossless mappings of these temporal sub-networks to a sequence of static networks and quantify the dissimilarity between them successively to obtain a dissimilarity function describing the changes between the successive temporal sub-networks. We extract the timescales of this function by taking its Fourier transform to identify its main frequency and harmonics. We focus here on applying this method to the detection of periodic changes in the link density and group structure of temporal networks. To this aim, first we consider synthetic networks in which we impose periodic variations of density and structure with tunable frequencies. We show that the method is able to retrieve the actual time scales of the networks. We then apply our method on several empirical temporal networks presenting periodic dynamics. In each case, the method captures correctly the system's main characteristic times, which could most often not be extracted by simple measures of the network overall activity. Our work opens the door to a better characterisation of the time scales of temporal networks, essential in the understanding of the dynamics of the underlying complex systems.

2 Methods

Let us consider a temporal network $G_T = (V, E_T, T)$ defined as a set V of nodes, and a set E_T of events over a time interval T measured in discrete time: each event $e(i, j, t) \in E_T$ describes a temporal interaction between two nodes $(i, j) \in V \times V$ at a certain time $t \in T$.

Temporal sub-networks. With such a temporal network as an input, we first extract a sequence of temporal sub-networks of G_T by using sliding windows of length Δt_w and stride t_w (shift between the start of successive windows). Specifically, the m^{th} sub-network G_T^m is composed of the nodes of V and of the subset E_{T^m} of events of E_T taking place in the time interval starting at time $m * t_w$ and ending at $m * t_w + \Delta t_w$:

$$G_T^m = (V, E_{T^m}, T^m = [m * t_w : m * t_w + \Delta t_w]) \quad \text{for} \quad m \in \mathbb{N} \quad \text{and} \quad T^m \subseteq T. \quad (1)$$

Based on this definition we can obtain a sequence of temporal sub-networks G_T^m to compute a dissimilarity function characterising the dynamical changes in the structure and the overall activities present in the original temporal network G_T . More precisely, we want to compute the dissimilarity between consecutive sub-networks, G_T^m and G_T^{m+1} .

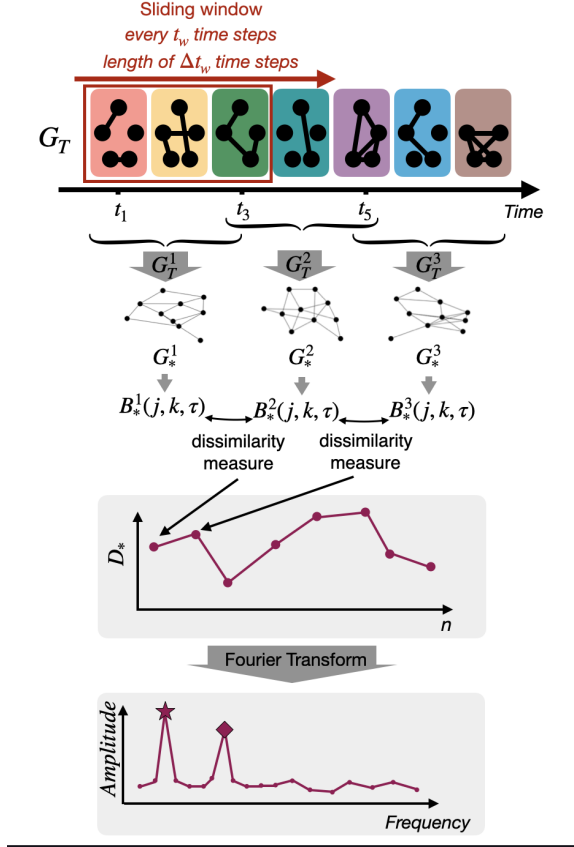


Figure 1: Methodology pipeline to measure the time scales of a temporal network G_T . From top to bottom: the initial temporal network is divided into sub-temporal networks through a sliding window. The m^{th} sub-network is denoted G_T^m . A static representation of each sub-network (G_*^m) is generated through the method $*$. Each G_*^m is described by a 3-dimensional tensor $B_*^m(j, k, \tau)$ that encodes information about the paths and distances in the sub-network (see Appendix A). We compare consecutive tensors with a dissimilarity measure, obtaining the dissimilarity function D_* . Finally, we compute the Fourier transform of D_* and measure the frequencies of the main harmonics.

Static network representations. To this aim, we first map each temporal sub-network onto a static network representation using two different methods. Note that both of these representations are lossless and contain the exact same amount of information as the temporal network they represent:

- The *Supra-Adjacency (SA)* representation [37, 38] $G_{SA} = (V_{SA}, E_{SA})$ of a temporal network G_T is a static directed network, in which each node $v_{SA} \in V_{SA}$ represents a pair (node, time) of the original temporal network: the node $(i, t) \in V_{SA}$ denotes that the node $i \in V$ was active at time $t \in T$, i.e., had at least one interaction at t . A directed edge $e_{SA} \in E_{SA}$ between two nodes of V_{SA} , (i, t_a) and (j, t_b) (with $t_a < t_b$), encodes the fact that an information can propagate on G_T from node i at t_a to node j at t_b , without intermediary events. If $i = j$, this is possible if t_a and t_b are successive interaction times for i (there is no event involving i at times $t_a < t < t_b$). Edges of type $(i, t_a) \rightarrow (i, t_b)$ in E_{SA} thus simply correspond to following the successive interaction times of i in G_T . For $i \neq j$ instead, the event $(i, j, t_a) \in E_T$ results in two directed edges in E_{SA} : $(i, t_a) \rightarrow (j, t_b)$ and $(j, t_a) \rightarrow (i, t_c)$, where t_b (resp. t_c) is the first time after t_a in which j (resp. i) is active again. The direction of edges in G_{SA} respects the arrow of time, and the set of edges E_{SA} allows to preserve the information about all possible temporal paths of the original temporal network.

- The *Event-Graph (EG)* representation G_{EG} [39, 40] is a static weighted directed acyclic network representation of a temporal network. Each event in G_T is represented by a node in G_{EG} , and two nodes of G_{EG} are connected if the two corresponding events in G_T were adjacent [39], i.e., share at least one node (in V) and are consecutive. Each edge between two nodes in G_{EG} is directed along the direction of time (from the earlier event to the later one) and is weighted by the time difference between the two corresponding events. Consequently, G_{EG} encodes also all information of time respecting paths emerging in the original temporal network.

These representations can be applied to any temporal network. In particular we apply them to each temporal sub-network G_T^m defined above to map them into a sequence of static representations G_{SA}^m and G_{EG}^m . In the following, we use the symbol $*$ to refer to the static representation method: it replaces the abbreviation *SA* or *EG*, as every object from now on can be calculated using one method or the other.

Network dissimilarity function. As a next step we compute a dissimilarity function $D_*(m)$ between successive static networks, G_*^m and G_*^{m+1} , for each sequence of static representations $\{G_*^m, m = 1, \dots\}$. To this aim, we consider here an extension of the method of [41] that summarizes the properties of a network in a matrix where the element (k, l) gives the number of nodes that can reach k other nodes in l hops in the structure. As we originally deal with temporal networks, and as the nodes of the *SA* and *EG* representations do keep temporal information, we instead describe each G_*^m by a tensor $B_*^m(j, k, \tau)$, which gives the number of nodes in G_*^m from which one can reach, in two hops on G_*^m , other nodes of G_*^m involving j nodes, k events and τ timestamps of G_T^m . The dissimilarity function D_*^m is finally computed as the Kullback-Leibler divergence between B_*^m and B_*^{m+1} .

Fourier Transform of dissimilarity function. Each dissimilarity function D_* provides an overall signal that reflects the structural and activity changes in the original temporal network. It presents higher values when the network goes through larger and abrupt transformations and takes smaller values when the network is more stable or changing only gradually with time. It can thus provide insights into the time scales of dynamical changes in the original temporal network. In particular, periodic patterns of network changes can be revealed by taking the Fourier transform of the dissimilarity function, which should present harmonics at the characteristic frequencies of the temporal network. More precisely, we compute the discrete-time Fourier transform of D_* defined as:

$$FT_k = \left| \sum_{j=0}^{N_{sample}} D_*(j) e^{i2\pi k j / N_{sample}} \right|, \quad (2)$$

where N_{sample} is the length of D_* and $k \in [0, N_{sample} - 1]$. The frequency corresponding to the k^{th} harmonic FT_k is $f_k = \frac{k}{t_w N_{sample}}$ where t_w is the time shift between two successive sub-networks G_T^m . The main harmonics of the *FT* function (appearing as the largest modes in the transformed function) correspond to the principal frequencies of the temporal network. Their inverse yield the characteristic time scales of the main periods present in the network dynamics.

In the following, we refer to the full methodology pipelines using respectively the *SA* and *EG* representations as the *SA – method* and *EG – method*. The whole generic pipeline is summarized in Figure 1.

3 Validation on synthetic data sets

To better understand the temporal properties that the above defined dissimilarity functions and their Fourier transforms can capture, we focus on synthetic temporal networks with controlled structural and temporal properties. In particular, we consider networks with tunable changes in activity (number of events per timestamp) and group structure. We utilise the Activity-Driven temporal network (ADN) model [42] for these purposes, defined by a set of N nodes $i = 1, \dots, N$, each having an intrinsic activity a_i taken from a given distribution. At each time step, node i becomes active

with probability ηa_i and, if active, establishes connections with m other nodes chosen randomly. Connections are erased after each time step thus the model does not present any memory nor correlations between time steps. Here we consider networks of size $N = 100$ with a power-law node activity distribution with minimum value $\epsilon = 0.001$ and parameters $\gamma = 1.8$, $m = 4$, $\eta = 4$ and $|T| = 9200$.

Using these parameters as baseline, we build three types of periodically varying temporal networks, to model the following settings:

- *Change of activity*: we simulate an ADN in which the density of edges varies periodically in time. We assign to each node i two activity values a_i^1 and a_i^2 , respectively extracted from two power-law distributions with exponents $\gamma_1 = 1.8$ and $\gamma_2 = 2.8$. We then alternate periodically (and synchronously for all nodes) between the two activity values, with a period T_a . This results in periodic changes in the overall activity of the network, as illustrated in Figure 2a.
- *Change of grouping*: we consider an ADN model of $N = 100$ nodes forming groups of 5 nodes each, and we periodically alternate, with a period of T_g , between time intervals in which connections are made at random with no restriction as in the baseline and intervals in which only connections within groups are allowed. The average activity is kept constant over time (Figure 2b).
- *Change of activity and grouping*: finally, we consider an ADN in which both activity and group structure change periodically over time, by combining the previous two mechanisms, each with its own period, respectively T_a and T_g (see Figure 2c).

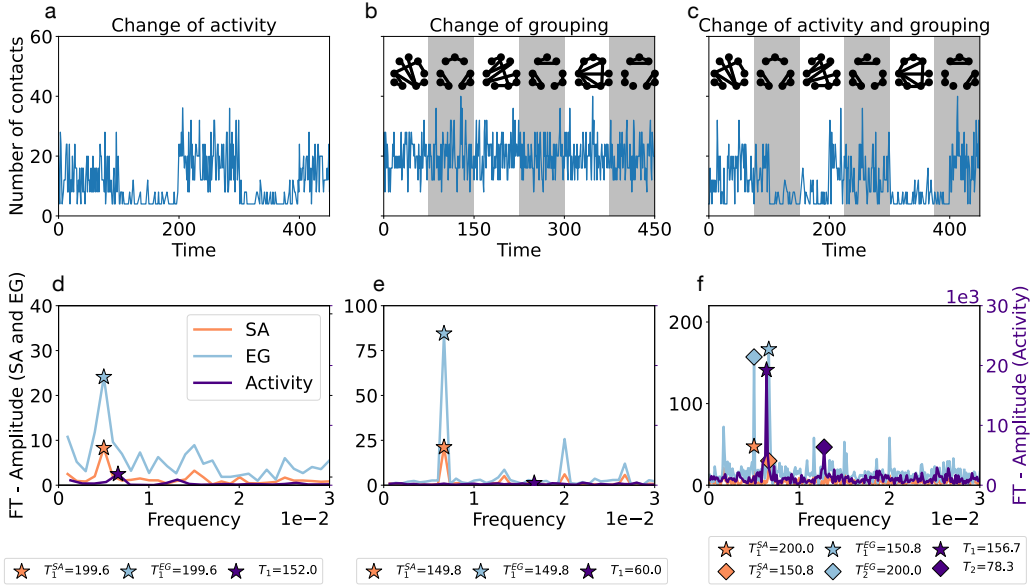


Figure 2: Schematic representation of three settings simulated with the Activity-Driven temporal network model with periodic changes of parameters ($N = 100$, $\epsilon = 0.001$, $\eta = 4$). (a) The *Change of activity* case presents networks with activity periods of $T_a = 200$; (b) the *Change of grouping* case presents recurrent structural changes with period $T_g = 150$; while (c) the *Change of activity and grouping* setting is defined as a mix of both dynamics. Panels (a-c) display the number of events as a function of time for a realization of each experiment; Gray areas in panels b and c indicate the intervals in which interactions can only occur within groups. Panels (d-f) depict the Fourier transforms of these networks obtained respectively through the SA-method and EG-method, as well as the Fourier transform of the activity timeline. The first and second harmonics of each Fourier transform are shown respectively with a star and a diamond symbol. In each case, the SA-method and EG-method are able to retrieve the correct period of the networks, while the Fourier transform of the activity signal fails in measuring temporal structural changes. In the *Change of activity and grouping* case, the SA-method identifies the frequency of activity changes as the main harmonic, while the EG-method detects the structural changes frequency as the dominant one.

For each case, we apply the SA and EG methods to compute the Fourier transforms of the resulting temporal networks. As a baseline method, we compute directly the Fourier transform of the activity function, that is measured as the link density at each time step of observation (see Figure 2). This is a simple summary metrics that describes the overall changes in the temporal network and can be computed for any system.

3.1 Results

The settings we consider involve either one or two types of periodic changes in the synthetic temporal networks: a periodic fluctuation in the amount of activity and/or in the network structure in terms of inter and intra group interactions. Our first goal is to investigate whether the SA- and EG-methods can uncover the corresponding periods T_a and T_g through the measure of the dominant frequencies in the associated Fourier transforms. As shown in Figure 2d and e, when only one type of periodic change is present, both methods are able to detect the corresponding period. It is evident from the depicted star symbols that indicate the largest mode in the frequency scale, correctly positioned at the right frequency corresponding to the period of the actual periodic changes. At the same time, the baseline method, computed as the FT of the activity timeline, strongly underperforms as compared to the other two methods. While in case of activity changes (see panel Figure 2d) it at least identifies approximately the value of the period, in case of periodical group changes it does not succeed to capture the rightful period at all. This was expected as in this case the overall activity does not reflect any periodicity but simply fluctuates randomly around a constant value.

When both types of periodic changes are present, an interesting distinction emerges between the results of the SA- and EG-methods. Indeed, both methods correctly detect the T_a and T_g periods as the first two dominant frequencies in the Fourier transform. However, in the SA-method the frequency describing the periodic activity changes is identified as the dominant frequency and the periodic group frequency to the second largest value ($T_1^{SA} = T_a = 200$, $T_2^{SA} = T_g = 150$ in Figure 2f), while this is reversed for the EG-method ($T_1^{EG} = T_g = 150$, $T_2^{EG} = T_a = 200$ in Figure 2f). These results suggest that the SA-method is more sensitive to periodic changes in activity, while the EG-method is more suited to detect periodic structural fluctuations. We also note that the FT of the baseline method yields as dominant timescales $T_1 = 156.7$ and $T_2 = 82.5$, the first one describing approximately the activity periods of the network, while the second one does not correspond to the period of either of the underlying processes.

To check the robustness of the proposed methods against the relative values of the periods, we further investigate this point by exploring systems with different values of T_a and T_g in the *Change of activity and grouping* setting. We generate 100 synthetic temporal networks for each pair of values (T_a, T_g), compute the dissimilarity function and Fourier Transforms of these realization, and extract the corresponding first two harmonics for each method (SA and EG).

Figure 3 summarizes the results by showing in each case the fraction of realizations which detected the periods of T_a, T_g correctly, or failed to detect any of them. These results demonstrate again that the SA-method identifies predominantly T_a (the activity change period) through the first harmonic and T_g (change of group structure) through the second, while the reverse is observed for the EG-method. Some deviations from this behaviour are observed at large values of the periods and/or when T_a and T_g are close to each other.

3.2 Parameter dependencies and limitations

Both the synthetic temporal networks and the analysis method involve some parameters. In particular, we explore their dependencies on the network size, temporal length and ratio between total temporal length and periods of changes T_a or T_g , with results presented in Appendix B. We observe that at large network size, both methods identify as main frequency a value corresponding the half value of the original period. Moreover, evidently, for correct time scale detection the observation period of the temporal network need to cover at least two full periods of any kind of changes.

The first step of our pipeline moreover involves the definition of sliding windows with stride t_w and length Δt_w . Naturally, these parameters affect the amount of information contained in each sub-temporal network and consequently influence the resulting dissimilarity function [43, 44, 45]. We

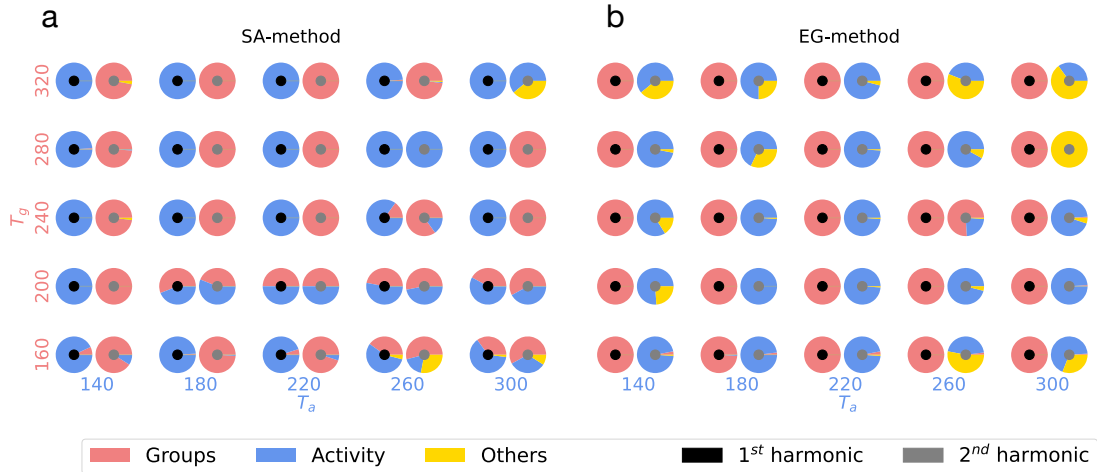


Figure 3: Periods corresponding to the two first harmonics measured through the SA-method (panel a) and the EG-method (panel b), for periodic synthetic temporal networks generated through the *Change of activity and grouping* setting ($N = 100$, $\epsilon = 0.001$, $\eta = 3$, $|T| = 9200$) with respective periods T_a (x-axis) and T_g (y-axis). For each pair of values (T_a, T_g) , we generate 100 realizations of the temporal network and apply the SA- and EG-method to extract the two main harmonics. We show in blue around a small black disk (resp. grey disk) the fraction of realizations in which the main frequency (resp. the second main) corresponds to T_a , in pink the fraction of cases in which it yields T_g , and in yellow the cases in which it corresponds to neither (we consider a tolerance of 10% for both periods). In most cases, both periods are correctly inferred, with the main frequency corresponding to T_a in the SA-method and to T_g in the EG-method.

explore the effect of these parameters in Appendix B, while keeping $t_w \leq \Delta t_w$ to have a non-zero overlap between successive time windows. We also ensure that the two parameters under study have values below the time span of the network's period (their maximum value is 20 while the period is 100).

As shown in Appendix B in Figure 10, the two methods show the best performance if the t_w stride is not too large and if Δt_w length is neither too high nor too small. If the time interval between two temporal sub-networks t_w is too high, we collect less information about the similarity between successive sliding windows. The dissimilarity function is then less precise and our methods perform less well to identify the characteristic temporal scales. Moreover, if Δt_w is too small, each sliding window contains too little information to obtain an accurate measure of the time-scale of the original network. On the opposite, if Δt_w is too large, each temporal sub-network may summarize too much information and lose the specific characteristic of the activity or the structure of the network on a certain time or interval of time. As an observation bias this could smooth dissimilarities between consecutive temporal network slices as they average too much information, and not because the network does not present significant changes through time.

It is also worth noticing that both methods measure systematically half of the period as dominant modes for very large values of t_w and Δt_w (Appendix B, Figure 10). In that case, every half-period of the network is covered by a small number of temporal sub-networks, leading to a lack of resolution in the dissimilarity function, in which only the peaks of dissimilarity at half-periods are well marked, leading to the detection of the half-period as typical timescale.

4 Applications on real networks

After validating our methods on synthetic networks with controlled properties, to explore further the capabilities of our methods, we consider empirical temporal networks representing different systems. We note that in such systems, in contrast to the cases studied above, several time scales, that correspond both to periodic or non-periodic fluctuations, may co-exist, as well as structural changes of different nature.

4.1 Data sets

We consider four temporal networks describing interactions of different nature, with various sizes and over different observation lengths. For more details about their temporal dynamics see Appendix C.

- *US middle school network*: this data set describes close proximity interactions between students of a middle school in the United States, during one day with temporal resolution of 20 seconds [46], recorded by Radio Frequency Identification (RFID) wearable devices. It involves several periods of class-times and inter-class breaks including two lunch periods, when students freely mix while changing classroom or eating together. The network consists of 591 nodes (each node corresponding to a student) and contains 473,755 records of pairwise temporal interactions between them.
- *Conference network*: these data also describe face-to-face contacts between individuals, with a temporal resolution of 20 seconds, obtained by RFID devices built on a different architecture [47]. The contacts were measured during a scientific conference, namely the IC2S2 conference that took place in Cologne (Germany) in 2017 [48]. Our observation period spans over the three first days of the conference, and records 229,536 temporal contacts between 274 participants. This data set, similar to the school data, is expected to show periodic behaviour both in terms of activity and structural changes, by reflecting the scheduled sessions and session-breaks of the conference.
- *Resistance game network*: it is an eye-contact network between participants of the Resistance game [49, 50], which is a role game where some of the players are hidden 'defeaters', and the goal of the other players is to uncover them. The game involves multiple rounds of around 4 minutes each, starting with a discussion involving every participant, and ending with a vote. The recorded network is built from directed events between participants who looked at each other at a given time t . The network is recorded between 8 individuals and contains 52,731 temporal interactions that we deem undirected for simplicity. This network provides an example where the interaction level should not reflect strong periodicity but the grouping of participants changes between each session.
- *US flight network*: this air-transportation network describes the direct flight connections between 278 airports in the US [51]. In our observation period we concentrate on 4 days of data that records 71,315 flights between the airports that we consider as undirected temporal interactions. This network is expected to show strong periodicities in activity, reflecting the daily recurrent flight schedules, while structural changes may not be strong as almost always the same airports are connected every day.

4.2 Results

After applying our pipeline on each data set using both the SA- and EG- and the baseline methods, in Figure 4 we depict the Fourier transforms of the obtained dissimilarity functions, with stars indicating the dominant frequencies. Interestingly, both the SA- and EG-methods identify the relevant timescales in most networks, while the baseline method consistently failed to detect them. For the *US middle school network*, both methods yield a timescale of about 46 minutes, coherent with the length of a class. Meanwhile, the baseline activity timeline FT would estimate the dominant frequency as corresponding to a period of 139 minutes. In the case of the *US flight network*, where the main changes are expected to be ruled by circadian fluctuations, both SA- and EG-methods also correctly identified periods of around 24 hours. This time-scale is also captured by the baseline method, but recognised only as its third largest harmonic. The two first harmonics are identified as periods of 5 and 10 minutes, which may correspond to the characteristic times between consecutive departures of planes from the same airport. The *Conference network* also presents strong signs of circadian changes of activity. This is reflected by all computed Fourier transforms, which show a harmonic corresponding to a period of about 24 hours for both the SA-method and the EG-method, captured as well by the baseline method. Finally, regarding the *Resistance game*, which presents only structural changes, the EG-method measures accurately the time-scales of periods characterising a

single round in the game, around 4 minutes. Since no periodic change of activities characterise this network, both the SA-method (more sensitive to activity changes) and the baseline method fail to identify any meaningful time-scale. The Fourier transform of the SA-method suggests the dominant mode to correspond to 0.53 minute, while the baseline method detects 13 minutes.

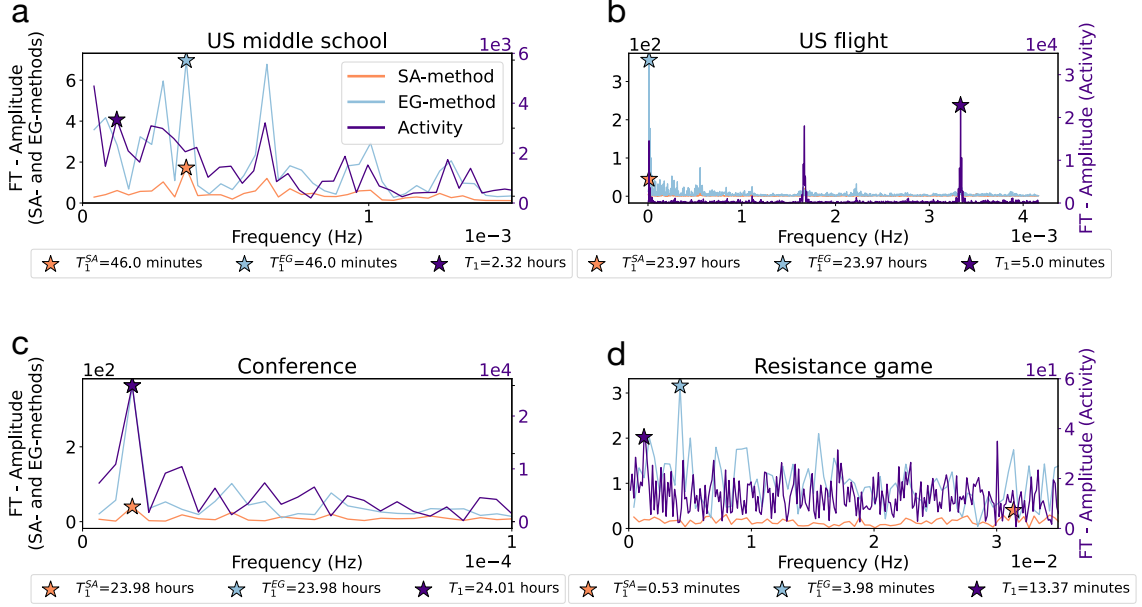


Figure 4: Fourier transforms of dissimilarity and activity functions of four real-world data sets (a) a US middle-school, (b) the US flight network, (c) a conference, and (d) the resistance game networks. Dissimilarity functions were calculated by the SA-method (in orange) and the EG-method (in blue), while results computed for the baseline model using activity signals are shown in purple. The highest harmonics are highlighted with a star symbol for each FT, and the corresponding values of the period is indicated below each panel. The parameters of the sliding windows ($t_w, \Delta t_w$) are (2 minutes, 5 minutes) for the *US middle school*, (1/3 minute, 1 minute) for the *Resistance game*, (2 minutes, 10 minutes) for the *US flight* and (2 minutes, 5 minutes) for the *Conference*.

4.3 Shuffling of the data

Empirical temporal network data entail structural and temporal correlations of different nature. To explore which of their characteristics play the main role in determining their relevant time-scales, a common method consists in shuffling the data to create randomized reference models [52] in which specific correlations are destroyed while others are preserved. In other words, through shuffling we create a sample from a uniformly sampled microcanonical ensemble of randomized networks, where certain network properties are kept constrained, while the networks are maximally random otherwise. Specifically, here we consider shuffling methods that remove the periodicity of the activity and/or of the group structure. In turn, we apply the SA- and EG-methods to compute the Fourier transforms of the shuffled data and check how these methods capture the modification of the time scales due to shuffling. We consider the following random reference models, following the canonical notations introduced in [52]:

- $P_p(\Gamma)$ shuffling: To remove both activity and structural correlations, we randomly shuffle the order of the temporal network snapshots, keeping fixed the structure of each snapshot. This procedure destroys any structural correlations between consecutive snapshots, removing the effects of structural reorganizations and randomizing also the activity timeline.
- P_τ shuffling: we rewire randomly all links in each snapshot of the temporal network. This is equivalent to creating a configuration random network [53] in each snapshot, with the same

number of nodes and edges as the original snapshot. The activity timeline is thus preserved while the group structure and its changes are removed.

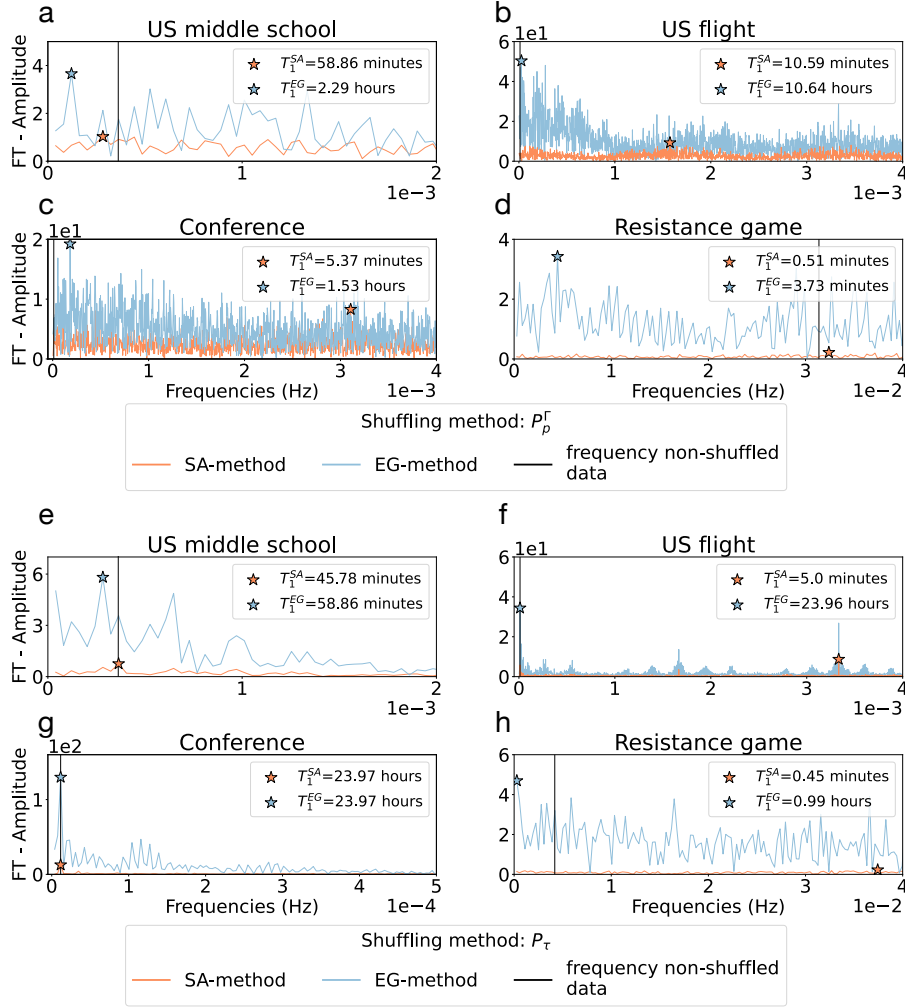


Figure 5: Fourier transform for the data sets US school, Resistance game, US flight and Conference networks shuffled using the two shuffling methods $P_p(\Gamma)$ (panels a-d) and P_t (panels e-h), obtained with the SA-method (orange curve) and the EG-method (blue curve). The period of each original data set is indicated with a black vertical line. For data shuffled using the $P_p(\Gamma)$ method, the original period is never recovered. In the case of the P_t shuffling instead, the SA- and EG methods still measure original periods if the network presents large activity changes (*US flight* and *Conference* data sets). In the case of the *US middle school* network, only the SA-method is able to assess the original time scale as this method performs better to detect activity changes. Finally, none of the method can measure the original period of the *Resistance game* network shuffled with the P_t method as it does not present any periodic variations.

Results are shown in Figure 5 for the four data sets and the two shuffling procedures. When the networks are shuffled with the $P_p(\Gamma)$ procedure (panels a-d), the original periods are not recovered, which is expected since the shuffling destroys any periodicity in the data.

However, when we shuffle the networks using the P_t method, which removes the structural effects but keeps the fluctuations in the overall activity, our methods present some capacity to identify the residual time scales in some of the data sets. In particular, two of the data sets present large periodic activity variations, i.e. the *US flight* and the *Conference* networks. After shuffling, these regular changes are still present, as the P_t method preserves their activity time line, while any other pattern has been destroyed by the shuffling. Consequently, we may still measure their original

circadian period from their P_τ -shuffled versions. Indeed, both the SA- and the EG-methods applied to the *Conference* network recover the dominant time scales, while in case of the *US flight* data set, the EG-method captures the expected time scale of around one day. We also find a time scale of 5 minutes with the SA-method applied to the *US flight* data set, which corresponds to another characteristic times of activity of this network (see Figure 4).

In contrast, both the SA- and the EG-methods miss the identification of the original time scales when applied on the P_τ -shuffled *Resistance game*. Since the original network has no periodic fluctuations in terms of activity, neither its shuffled counterpart present any regular changes in term of activity. Thus the detected time scales are only induced by some noise in the data.

Finally, the *US middle school* network presents activity variations that are not easily assessed even in the original network. Once shuffling with the P_τ method, only the SA-method, which is overall more sensitive to activity changes, retrieves the original period (≈ 46 minutes) in the shuffled network. The EG-method overestimates this time by detecting a period of $5 \approx 9$ minutes.

5 Conclusion

In this work, we have put forward a new methodology to uncover periodic time-scales in temporal networks. In our proposed pipeline, first we locally aggregate the original temporal network by using a sliding window to build a sequence of temporal sub-networks. Subsequently, we map these temporal sub-networks into a sequence of static networks, using known lossless higher-order temporal network representations, namely supra-adjacency matrices or event-graphs. We further extend a method for the comparison between the consecutive static network samples to define a dissimilarity function that reflects activity and structural changes in the original temporal network. Finally, we take the Fourier transform of the dissimilarity function to detect the relevant periodic time-scales from the dominant frequencies characterising the original network.

We have explored this pipeline, focusing on changes in the activity and group structure of temporal networks. Using synthetic data sets with prescribed changes, we have shown that while both methods are able to recover the time scales of the modelled periodic dynamics, they perform differently in the identification of changes in activity and structure. Specifically, the SA-method is more sensitive to overall activity changes while the EG-method captures better periodic structural fluctuations, which cannot instead be obtained through the FT of the activity timeline. We have also shown that these methods are able to highlight relevant periods in more complex empirical data sets.

The methodology presented here have certain limitations. First, its performance depends on some parameters of the aggregation method and the temporal network observed. The observation needs in particular to span a long enough interval: at least two periods of changes need to be observed. The sliding window parameters also have some impact on the performance: each temporal sub-network should encode enough information but should not be too long to average out relevant changes. The stride should be small enough to keep a reasonable temporal resolution and a substantial overlap between successive windows.

The proposed methodology pipeline opens the door to the investigation of several interesting extensions and research questions. Possible extensions of the present method could include the consideration of other static representations as well as other similarity measures between successive temporal sub-networks ¹, which could potentially be more sensitive to various types of structural changes of the temporal network. For instance, it would be interesting to explore whether changes in the instantaneous core-periphery structure [25] could be uncovered. Future work could also explore extensions to time-varying hypergraphs [54, 55] or the interaction between the detected time scales of the underlying temporal network and ongoing dynamical processes. Our work presents a proof of concept for a new methodological direction that will contribute to the better characterisation of time varying complex structures.

¹including the tensor portrait defined in Appendix A but considering different numbers of hops from each node.

Acknowledgment

We acknowledge support from the Agence Nationale de la Recherche (ANR) project DATAREDEX (ANR-19-CE46-0008). MK was supported by the CHIST-ERA project SAI: FWF I 5205-N; the SoBigData++ H2020-871042; the EMOMAP CIVICA projects and the National Laboratory for Health Security, Alfréd Rényi Institute, RRF-2.3.1-21-2022-00006.

A Comparing temporal networks

An important step in our methodology is to quantify the similarity between successive temporal sub-networks. We first map each temporal sub-network to a static one, as described in the main text, and compare these static representations. To this aim, we adapt a method proposed by Bagrow and Boltt [41], which allows to compare static networks at multiple scales. The first step of this method is to compute, for each static network, its “portrait” B defined as

$$B_{l,k} = \text{number of nodes which have } k \text{ nodes at distance } l .$$

The dissimilarity between two networks is then given by the Kullback-Leibler divergence between their respective portraits.

In our case, the static networks that we need to compare are representations of temporal networks, with either the Supra-Adjacency or the Event-Graph method, noted G_*^m . Nodes and edges in these networks contain information about nodes, interactions and times of the original temporal network. To take this into account, we adapt and modify the definition of network portrait, and define the tensor portrait of G_*^m by relying on $BD_*^m(j, k, \tau)$ which is the number of nodes of G_*^m which can reach, in two hops, j nodes, k events and τ timestamps of the original temporal network. In other words, we consider for each node of the static representation G_*^m its ego-network at distance 2, and count the number of distinct nodes, timestamps and events of the original temporal network G_T^m involved. We then collect this information for all nodes of G_*^m and summarize the resulting histogram as the portrait BD_*^m . We illustrate this method to compute the tensor portrait BD_*^m in Figure 6.

We also note that the static representation of the temporal networks are directed, with edge directions following the arrow of time. The ego-network of a node of the static representation involves only future timestamps and events. To take also into account how each node can receive information from events in the past, we create for each G_*^m its reversed version $G_{*,R}^m$ by inverting the direction of each edge of the representation and compute its portrait BR_*^m . We then obtain the final tensor B_*^m by summing BD_*^m and BR_*^m .

Finally, we compute the dissimilarity between each pair of consecutive tensors B_*^m and B_*^{m+1} , as their Kullback-Leibler divergence (if the two tensors B_*^m and B_*^{m+1} differ in size, we adjust the size of the smaller one to the size of the biggest one by filling the missing entries with zeros). The dissimilarity function is defined as:

$$D_*(m) = KL(B_*^m, B_*^{m+1}) \quad \text{for } m \in \mathbb{N}$$

Note that, in the event of an empty network, the Kullback-Leibler divergence is not defined. We then assign one single event to the corresponding empty temporal sub-network G_T^m .

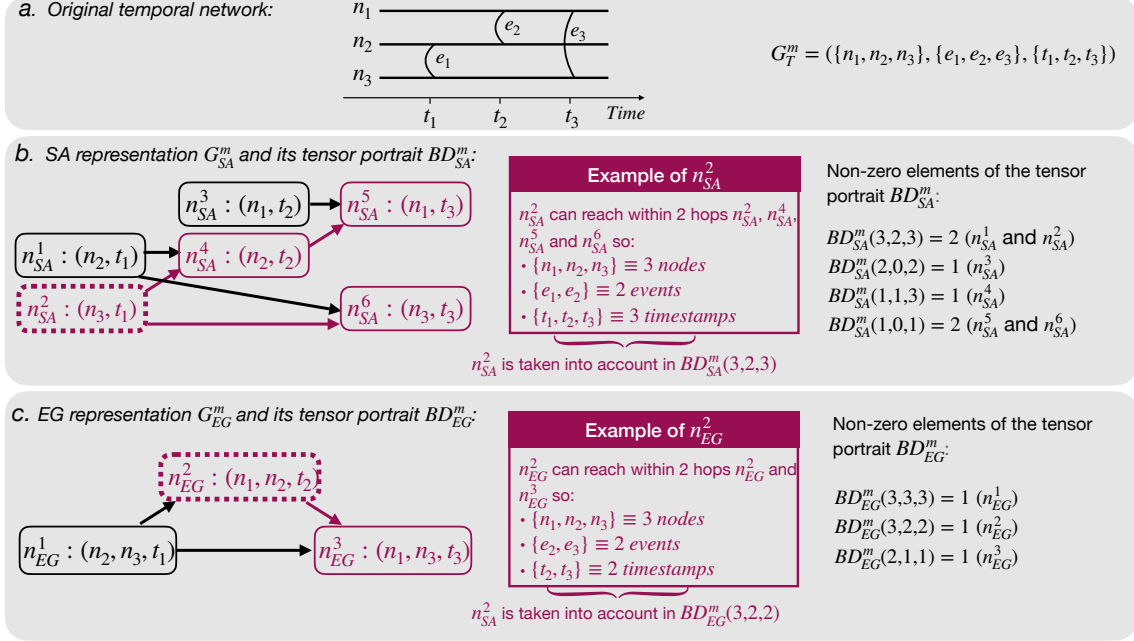


Figure 6: Sketch of the method to compute the tensor portraits BD_*^m of the temporal network G_T^m displayed in panel a. The static SA and EG representations G_{SA}^m and G_{EG}^m are shown respectively in panels b and c. We first evaluate the number of nodes, events and timestamps from the temporal network accessible within two hops from each node of the static networks. We illustrate the computation for n_*^2 (purple highlight). We then count the number of nodes of the static representation that can reach j nodes, k events and τ timestamps of the original temporal network to compute the element $BD_*^m(j, k, \tau)$ of the tensor portrait.

B Sensitivity analysis: size and length of the temporal network, sliding window parameters

To evaluate the reliability of our results, we perform a sensitivity analysis on the parameters of the experiments *Change of activity* and *Change of grouping*. We change one parameter in both experiments while keeping the other constant ($N = 100$, $\epsilon = 0.001$, $\eta = 45$, μ oscillating between 1.8 and 2.8 for the *Change of activity* and $\mu = 2.8$ for *Change of grouping*, $T_a = T_g = 100$, $|T|$ is adjusted to have 12 periods, $\Delta t_w = 5$ and $t_w = 2$).

When we vary the number of nodes of the networks (Figure 7), the original period is almost always measured properly except when the number of nodes is high. In that case, the measured period is 50 (corresponding to a frequency of 0.02), which is half of the original period. In fact, when the networks change from a high-activity state to a low-activity state, we observe a peak in the dissimilarity function. This situation happens twice in a period: when changing from low to high and from high to low activity. The measured period is then the half period (Note that this happens at all sizes, and the half-period is indeed always recovered as one of the harmonics, but it seems here to become dominant at large sizes).

The same analysis has been realized by changing the length of the period (Figure 8) and in every case, the original period is correctly measured: the length of the period does not influence the observation. Instead, when we change the number of periods observed (Figure 9), we observe that we need a minimum of 2 periods to measure the original time scale.

We finally study the influence of the parameters of the sliding window t_w and Δt_w on the results. In Figure 10, we compute the Fourier Transform of the AD network with the SA-method and the EG-method having different parameters t_w and Δt_w . The correct period (100) is properly measured if t_w and Δt_w are not too large.

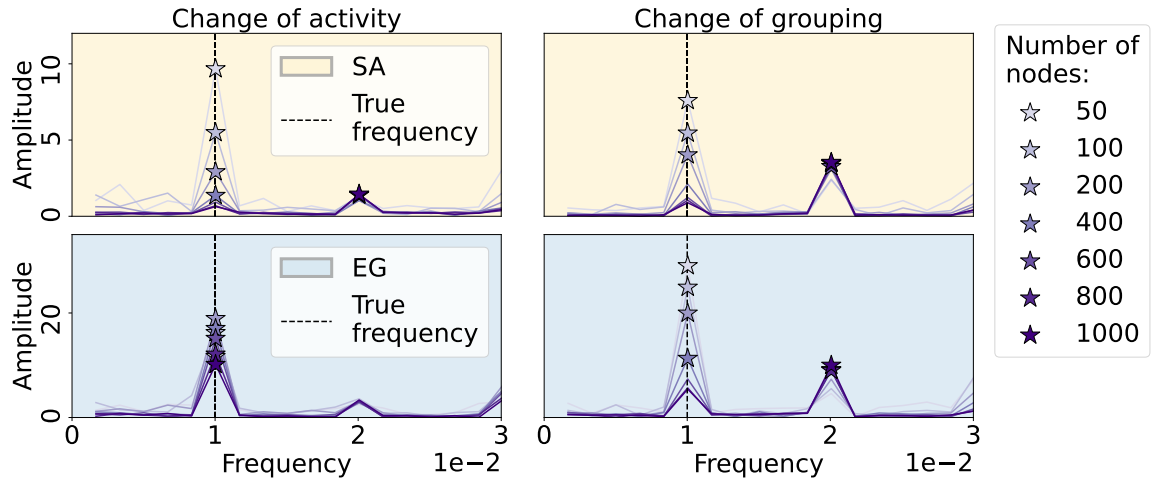


Figure 7: Fourier transforms of the temporal network from the *Change of activity* experiment (left column) and the *Change of grouping* experiment (right column) measured from the SA-method (yellow background) and the EG-method (blue background). The number of nodes of the AD networks varies from 50 to 1000. The correct frequencies are indicated with vertical dashed lines. Those original periods are well-measured in the majority of the cases. However, when the number of nodes is too important, the method measures the semi-period.

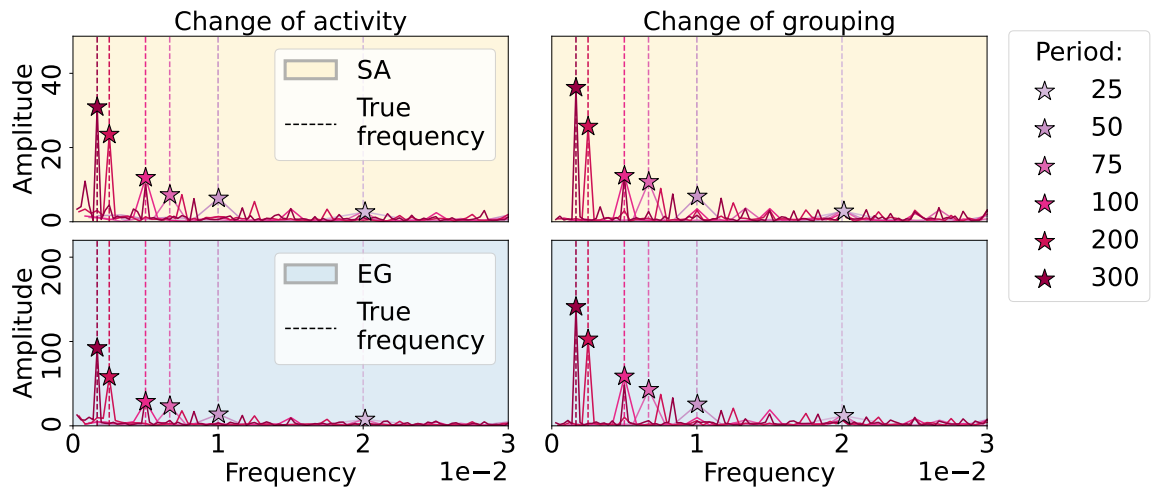


Figure 8: Fourier transforms of the temporal network from the *Change of activity* experiment (left column) and the *Change of grouping* experiment (right column) measured from the SA-method (yellow background) and the EG-method (blue background). The period varies from 25 to 300. The correct frequencies are indicated with vertical dashed lines and are here always well recovered.

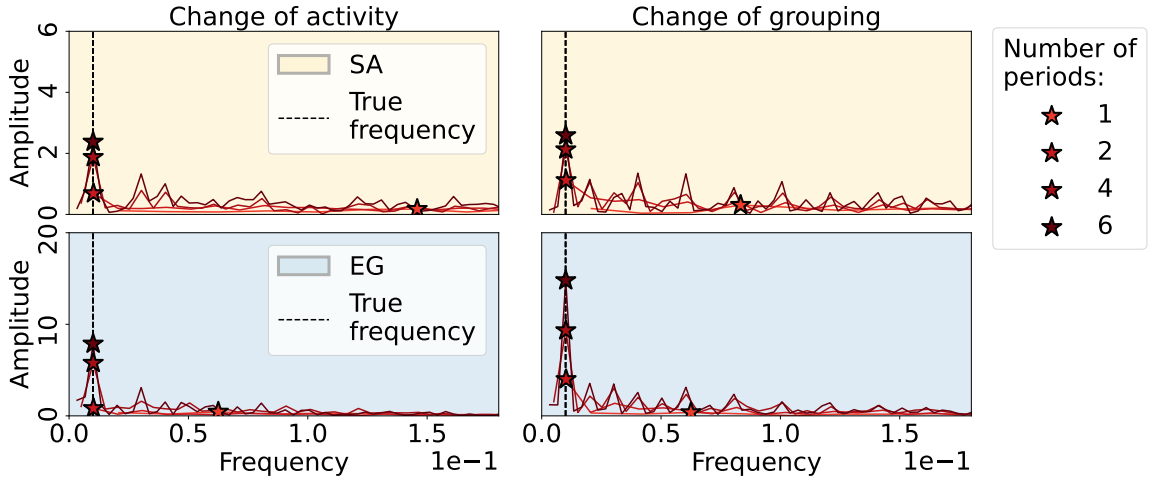


Figure 9: Fourier transforms of the temporal network from the *Change of activity* experiment (left column) and the *Change of grouping* experiment (right column) measured from the SA-method (yellow background) and the EG-method (blue background). The number of periods of the AD networks observed during T varies from 1 to 6. The correct frequencies are indicated with vertical dashed lines. Those proper periods are well-measured as long as the data set contains at least two periods.

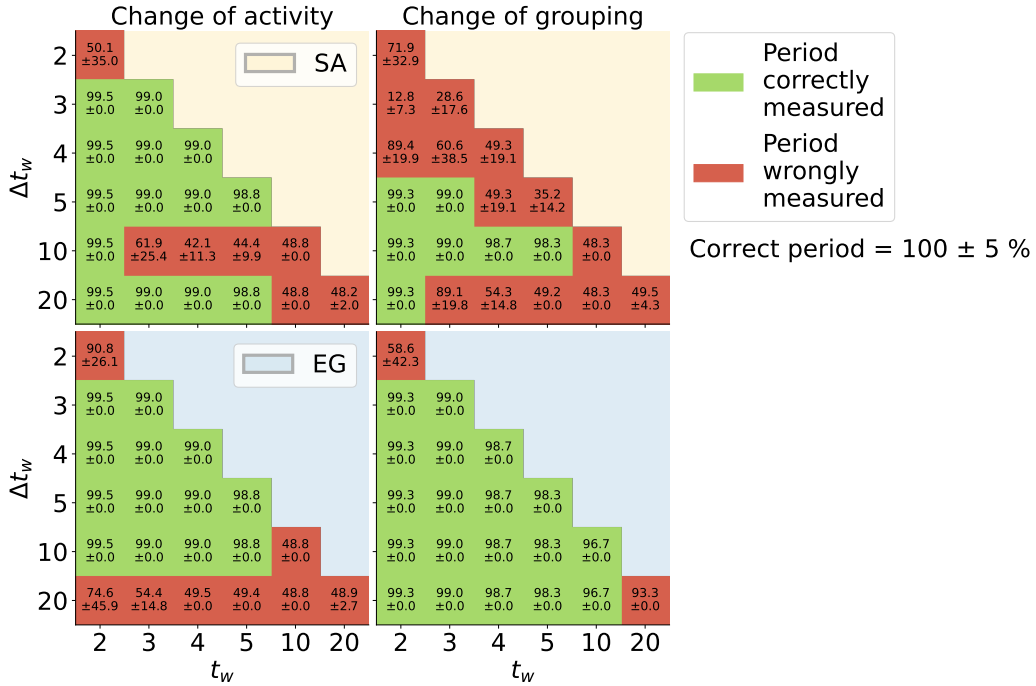


Figure 10: Period measured through the SA-method (orange background) and the EG-method (blue background) for the *Change of activity* experiment (first column) and the *Change of grouping* experiment (second column). We change the parameters of the sliding window: the x-axis presents different values of the stride t_w and the y-axis different values of time-window lengths (Δt_w). The period of the initial networks is 100 and the results are averaged over 10 realisations. The results are displayed as the average period over the different realisations \pm the standard deviation.

C Empirical data

We observe the changes of activity over time of the empirical networks for the four data sets (Figure 11). The *US school* presents periodic patterns, varying from low contact periods when the students are in class to high contact periods when there is a recreational time. The *US flight* and *Conference* networks have circadian patterns as there are respectively less flights and less contacts at night. Finally, the *Resistance game* does not present any periodic change in its activity as every player of the game is looking at someone else at each time step.

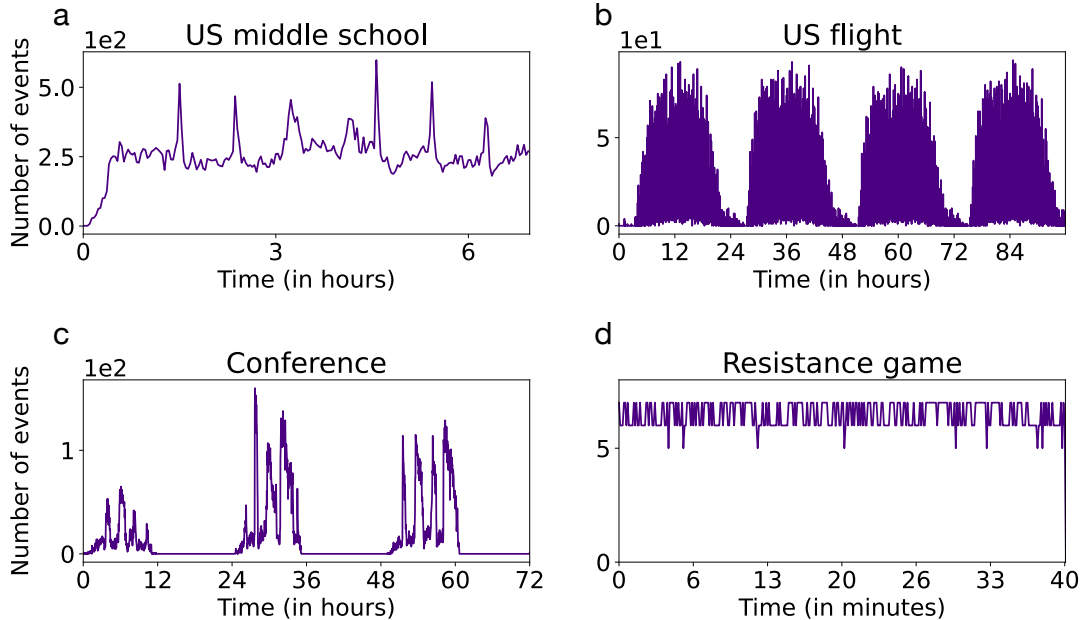


Figure 11: Number of events as a function of time for the four data sets: the *US school* (panel a), the *US flight* (panel b), the *Conference* (panel c) and the *Resistance game* (panel d). The *US school* network contains high activity periods during recreational moments of the students’ day, while the *US flight* and the *Conference* networks present circadian patterns. The *Resistance game* network does not have particular periodic activity changes.

References

- [1] Petter Holme and Jari Saramäki. Temporal networks. *Physics reports*, 519(3):97–125, 2012.
- [2] Petter Holme. Modern temporal network theory: a colloquium. *The European Physical Journal B*, 88:1–30, 2015.
- [3] Naoki Masuda and Renaud Lambiotte. *A guide to temporal networks*. World Scientific, 2016.
- [4] Alain Barrat and Ciro Cattuto. Temporal networks of face-to-face human interactions. *Temporal networks*, pages 191–216, 2013.
- [5] Sune Lehmann. Fundamental structures in temporal communication networks. *Temporal Network Theory*, pages 25–48, 2019.
- [6] Mohammed Saqr and Sonsoles López-Pernas. The why, the what and the how to model a dynamic relational learning process with temporal networks. In *Proceedings of the NetSciLA22 workshop*, 2022.

- [7] Kristian Trøjelsgaard and Jens M Olesen. Ecological networks in motion: Micro-and macroscopic variability across scales. *Functional Ecology*, 30(12):1926–1935, 2016.
- [8] Mohammad Mehdi Hosseinzadeh, Mario Cannataro, Pietro Hiram Guzzi, and Riccardo Dondi. Temporal networks in biology and medicine: a survey on models, algorithms, and tools. *Network Modeling Analysis in Health Informatics and Bioinformatics*, 12(1):10, 2022.
- [9] Nam Huynh and Johan Barthelemy. A comparative study of topological analysis and temporal network analysis of a public transport system. *International Journal of Transportation Science and Technology*, 11(2):392–405, 2022.
- [10] Mohamed Salama, Mohamed Ezzeldin, Wael El-Dakhakhni, and Michael Tait. Temporal networks: A review and opportunities for infrastructure simulation. *Sustainable and resilient infrastructure*, 7(1):40–55, 2022.
- [11] A. Barrat, M. Barthélemy, and A. Vespignani. *Dynamical Processes on Complex Networks*. Cambridge University Press, 2008.
- [12] Dan Braha and Yaneer Bar-Yam. Time-dependent complex networks: Dynamic centrality, dynamic motifs, and cycles of social interactions. In *Adaptive networks: Theory, models and applications*, pages 39–50. Springer, 2009.
- [13] Raj Kumar Pan and Jari Saramäki. Path lengths, correlations, and centrality in temporal networks. *Physical Review E*, 84(1):016105, 2011.
- [14] Aming Li, Sean P Cornelius, Y-Y Liu, Long Wang, and A-L Barabási. The fundamental advantages of temporal networks. *Science*, 358(6366):1042–1046, 2017.
- [15] Dan Braha and Yaneer Bar-Yam. From centrality to temporary fame: Dynamic centrality in complex networks. *Complexity*, 12(2):59–63, 2006.
- [16] Eduardo C Costa, Alex B Vieira, Klaus Wehmuth, Artur Ziviani, and Ana Paula Couto Da Silva. Time centrality in dynamic complex networks. *Advances in Complex Systems*, 18(07n08):1550023, 2015.
- [17] Albert-Laszlo Barabasi. The origin of bursts and heavy tails in human dynamics. *Nature*, 435(7039):207–211, 2005.
- [18] Márton Karsai, Kimmo Kaski, and János Kertész. Correlated dynamics in egocentric communication networks. *Plos one*, 7(7):e40612, 2012.
- [19] Talayeh Aledavood, Sune Lehmann, and Jari Saramäki. Digital daily cycles of individuals. *Frontiers in Physics*, 3:73, 2015.
- [20] Paolo Bajardi, Alain Barrat, Fabrizio Natale, Lara Savini, and Vittoria Colizza. Dynamical patterns of cattle trade movements. *PloS one*, 6(5):e19869, 2011.
- [21] Lauri Kovanen, Márton Karsai, Kimmo Kaski, János Kertész, and Jari Saramäki. Temporal motifs in time-dependent networks. *Journal of Statistical Mechanics: Theory and Experiment*, 2011(11):P11005, 2011.
- [22] Antonio Longa, Giulia Cencetti, Bruno Lepri, and Andrea Passerini. An efficient procedure for mining egocentric temporal motifs. *Data Mining and Knowledge Discovery*, 36(1):355–378, Jan 2022.
- [23] Laetitia Gauvin, André Panisson, and Ciro Cattuto. Detecting the community structure and activity patterns of temporal networks: a non-negative tensor factorization approach. *PloS one*, 9(1):e86028, 2014.
- [24] Peter Csermely, András London, Ling-Yun Wu, and Brian Uzzi. Structure and dynamics of core/periphery networks. *Journal of Complex Networks*, 1(2):93–123, 2013.

- [25] Nicola Pedreschi, Christophe Bernard, Wesley Clawson, Pascale Quilichini, Alain Barrat, and Demian Battaglia. Dynamic core-periphery structure of information sharing networks in entorhinal cortex and hippocampus. *Network Neuroscience*, 4(3):946–975, 2020.
- [26] Nicola Pedreschi, Demian Battaglia, and Alain Barrat. The temporal rich club phenomenon. *Nature Physics*, 18(8):931–938, 2022.
- [27] Edoardo Galimberti, Alain Barrat, Francesco Bonchi, Ciro Cattuto, and Francesco Gullo. Mining (maximal) span-cores from temporal networks. In *Proceedings of the 27th ACM international Conference on Information and Knowledge Management*, pages 107–116, 2018.
- [28] Jari Saramäki and Esteban Moro. From seconds to months: an overview of multi-scale dynamics of mobile telephone calls. *The European Physical Journal B*, 88:1–10, 2015.
- [29] Valeria Gelardi, Joël Fagot, Alain Barrat, and Nicolas Claidière. Detecting social (in) stability in primates from their temporal co-presence network. *Animal Behaviour*, 157:239–254, 2019.
- [30] Naoki Masuda and Petter Holme. Detecting sequences of system states in temporal networks. *Scientific reports*, 9(1):1–11, 2019.
- [31] Julie Fournet and Alain Barrat. Contact patterns among high school students. *PloS one*, 9(9):e107878, 2014.
- [32] Maxime Lucas, Arthur Morris, Alex Townsend-Teague, Laurent Tichit, Bianca Habermann, and Alain Barrat. Inferring cell cycle phases from a partially temporal network of protein interactions. *Cell Reports Methods*, 3(2), 2023.
- [33] Juliette Stehlé, Nicolas Voirin, Alain Barrat, Ciro Cattuto, Lorenzo Isella, Jean-François Pinton, Marco Quagiotto, Wouter Van den Broeck, Corinne Régis, Bruno Lina, et al. High-resolution measurements of face-to-face contact patterns in a primary school. *PloS one*, 6(8):e23176, 2011.
- [34] Richard K Darst, Clara Granell, Alex Arenas, Sergio Gómez, Jari Saramäki, and Santo Fortunato. Detection of timescales in evolving complex systems. *Scientific reports*, 6(1):39713, 2016.
- [35] Kashin Sugishita and Naoki Masuda. Recurrence in the evolution of air transport networks. *Scientific reports*, 11(1):1–15, 2021.
- [36] Lucas Lacasa, Jorge P Rodriguez, and Victor M Eguiluz. Correlations of network trajectories. *Physical Review Research*, 4(4):L042008, 2022.
- [37] Eugenio Valdano, Luca Ferreri, Chiara Poletto, and Vittoria Colizza. Analytical computation of the epidemic threshold on temporal networks. *Physical Review X*, 5(2):021005, 2015.
- [38] Koya Sato, Mizuki Oka, Alain Barrat, and Ciro Cattuto. Dyane: dynamics-aware node embedding for temporal networks. *arXiv preprint arXiv:1909.05976*, 2019.
- [39] Mikko Kivelä, Jordan Cambe, Jari Saramäki, and Márton Karsai. Mapping temporal-network percolation to weighted, static event graphs. *Scientific reports*, 8(1):1–9, 2018.
- [40] Andrew Mellor. Event graphs: Advances and applications of second-order time-unfolded temporal network models. *Advances in Complex Systems*, 22(03):1950006, 2019.
- [41] James P Bagrow and Erik M Bollt. An information-theoretic, all-scales approach to comparing networks. *Applied Network Science*, 4(1):1–15, 2019.
- [42] Nicola Perra, Bruno Gonçalves, Romualdo Pastor-Satorras, and Alessandro Vespignani. Activity driven modeling of time varying networks. *Scientific reports*, 2(1):1–7, 2012.
- [43] Rajmonda Sulo, Tanya Berger-Wolf, and Robert Grossman. Meaningful selection of temporal resolution for dynamic networks. In *Proceedings of the Eighth Workshop on Mining and Learning with Graphs*, pages 127–136, 2010.

- [44] Gautier Krings, Márton Karsai, Sebastian Bernhardsson, Vincent D Blondel, and Jari Saramäki. Effects of time window size and placement on the structure of an aggregated communication network. *EPJ Data Science*, 1(1):1–16, 2012.
- [45] Mikko Kivelä and Mason A Porter. Estimating interevent time distributions from finite observation periods in communication networks. *Physical Review E*, 92(5):052813, 2015.
- [46] Damon JA Toth, Molly Leecaster, Warren BP Pettey, Adi V Gundlapalli, Hongjiang Gao, Jeanette J Rainey, Amra Uzicanin, and Matthew H Samore. The role of heterogeneity in contact timing and duration in network models of influenza spread in schools. *Journal of The Royal Society Interface*, 12(108):20150279, 2015.
- [47] Ciro Cattuto, Wouter Van den Broeck, Alain Barrat, Vittoria Colizza, Jean-François Pinton, and Alessandro Vespignani. Dynamics of person-to-person interactions from distributed rfid sensor networks. *PloS one*, 5(7):e11596, 2010.
- [48] Mathieu Génois, Maria Zens, Marcos Oliveira, Clemens M Lechner, Johann Schaible, and Markus Strohmaier. Combining sensors and surveys to study social interactions: A case of four science conferences. *Personality Science*, 4:1–24, 2023.
- [49] Chongyang Bai, Srijan Kumar, Jure Leskovec, Miriam Metzger, Jay F Nunamaker Jr, and VS Subrahmanian. Predicting the visual focus of attention in multi-person discussion videos. In *IJCAI*, pages 4504–4510, 2019.
- [50] Srijan Kumar, Chongyang Bai, VS Subrahmanian, and Jure Leskovec. Deception detection in group video conversations using dynamic interaction networks. In *ICWSM*, pages 339–350, 2021.
- [51] Bureau of transportation statistics, bureau of transportation statistics website (2017).
- [52] Laetitia Gauvin, Mathieu Génois, Márton Karsai, Mikko Kivelä, Taro Takaguchi, Eugenio Valdano, and Christian L Vestergaard. Randomized reference models for temporal networks. *SIAM Review*, 64(4):763–830, 2022.
- [53] Mark Newman. *Networks*. Oxford university press, 2018.
- [54] F. Battiston, G. Cencetti, I. Iacopini, V. Latora, M. Lucas, A. Patania, J.-G. Young, and G. Petri. Networks beyond pairwise interactions: Structure and dynamics. *Phys. Rep.*, 874:1–92, 2020.
- [55] F. Battiston, E. Amico, A. Barrat, G. Bianconi, G. Ferraz de Arruda, B. Franceschiello, I. Iacopini, S. Kéfi, V. Latora, Y. Moreno, M. Murray, T. Peixoto, F. Vaccarino, and G. Petri. The physics of higher-order interactions in complex systems. *Nat. Phys.*, 17(10):1093–1098, 2021.